
CHAPTER 12

GROUND ECHO

Richard K. Moore
The University of Kansas

12.1 INTRODUCTION

Radar ground return is described by σ^0 , the differential scattering cross section, or scattering coefficient (scattering cross section per unit area), rather than by the total scattering cross section σ used for discrete targets.¹ Since the total cross section σ of a patch of ground varies with the illuminated area and this is determined by the geometric radar parameters (pulse width, beamwidth, etc.), σ^0 was introduced to obtain a coefficient independent of these parameters.

Use of a differential scattering cross section implies that the return from the ground is contributed by a large number of scattering elements whose phases are independent. This is primarily because of differences in distance that, although small fractions of total distance, are many wavelengths. Superposition of power is possible for the computation of average returns. If this condition is not applicable to a particular ground target, the differential-scattering-cross-section concept has no meaning for that target. For example, a very-fine-resolution radar might be able to resolve a part of a car; the smooth surfaces on the car would not be properly represented by σ^0 . On the other hand, a coarser radar might look at many cars in a large parking lot, and a valid σ^0 for the parking lot could be determined.

If a region illuminated at one time by a radar contains n scattering elements and the above criterion is satisfied so that power may be added, the radar equation becomes

$$P_r = \sum_i^n \frac{P_{ii} G_{ii} A_r \sigma_i}{(4\pi R_i^2)^2} = \sum_i^n \frac{P_{ii} G_{ii} A_r (\sigma_i / \Delta A_i) \Delta A_i}{(4\pi R_i^2)^2}$$

Here ΔA_i is an element of surface area, and P_{ii} , G_{ii} , and A_{ri} are values of P , G , and A_r appropriate for an element at the location of ΔA_i . The factor in parentheses in the numerator of the right-hand expression is the incremental scattering cross section for element i , but this concept is meaningful only in an average. Thus the average power returned is given by

$$P_r = \sum_i^n \frac{P_{ti} G_{ti} A_{ri} \sigma^0 \Delta A_i}{(4\pi R_i^2)^2}$$

Here σ^0 has been used to denote the average value of $\sigma_i/\Delta A_i$. In this formulation, we may pass in the limit from the finite sum to the integral given by

$$\bar{P}_r = \frac{1}{(4\pi)^2} \int_{\text{Illuminated area}} \frac{P_t G_t A_r \sigma^0 dA}{R^4} \quad (12.1)$$

The bar over P_r implies the average value. This integral is not really correct, for there is a minimum size for real, independent scattering centers. Nevertheless, the concept is widely used and is applicable as long as the illuminated area is large enough to contain many such centers.

Figure 12.1 illustrates the geometry associated with Eq. (12.1). Note that, for a rectangular pulse, P_t is either zero or the peak transmitter power but, for other pulse shapes, the variation with t (or R) is significant. Actual pulses are often approximated by rectangular pulses with widths equal to their half-power widths. Real pulses cannot be rectangular after passing through real receiver bandwidths. The transmitting-antenna gain and receiving-antenna aperture are functions of the elevation and azimuth angles:

$$G_t = G_t(\theta, \phi) \quad A_r = A_r(\theta, \phi) \quad (12.2a)$$

The differential scattering cross section itself is a function of both *look angle* and ground location:

$$\sigma^0 = \sigma^0(\theta, \phi, \text{location}) \quad (12.2b)$$

The integral of Eq. (12.1) must be inverted when σ^0 is measured. With narrow beams and short pulses the inversion is relatively easy, but with the wider beams and longer pulses used in many measurements the values obtained are sometimes poorly defined.

Some authors² use a scattering cross section per unit projected area rather than per unit ground area. Figure 12.2 illustrates by a *side view* the difference between ground area and projected area. The ground area is proportional to Δp , and the projected area is smaller. Thus,

$$\sigma^0 A = \gamma d(\text{projected area}) = \gamma \cos \theta dA \quad (12.3)$$

or
$$\sigma^0 = \gamma \cos \theta$$

Since both γ and σ^0 are called scattering coefficients, readers of the literature must be especially careful to determine which is being used by a particular author.

Radar astronomers use a different σ :³

$$\sigma = \frac{\text{total return power from entire surface}}{\text{power returned from perfect isotropic sphere of same radius}} \quad (12.4)$$

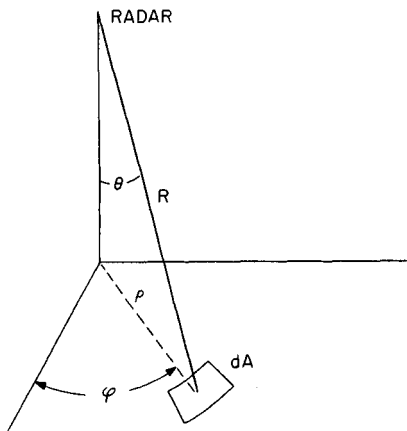


FIG. 12.1 Geometry of the radar equation.

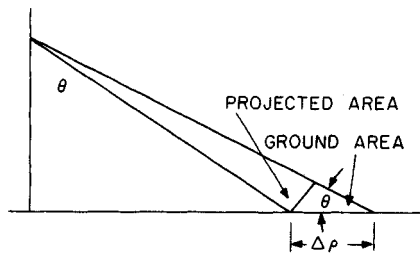


FIG. 12.2 Ground area and projected area.

The resulting value for σ is usually much smaller than σ^0 for the planet at vertical incidence and is larger than the values of σ^0 near grazing incidence (return from the limb of the planet).

Relative Importance of Theory and Empiricism. The theory of radar ground return has been the subject of many publications. The various theories, insofar as they can be confirmed by experiment, provide bases for judging the effects of variations in the dielectric properties of the ground, of the roughness of the ground and nature of vegetative or snow cover, of radar wavelength, and of angle of incidence. Viewed as aids to insight, radar ground-return theories can be extremely useful.

The validity of any ground-return theory must depend on the mathematical model used to describe the surface, as well as on the approximations required to obtain answers. Even the simplest ground surface, the sea, is extremely difficult to describe accurately; it is homogeneous to beyond the skin depth, contains relatively modest slopes, and (except for spray) has no part above another part of the surface. At grazing angles, shadowing of one wave by another might occur. Land surfaces are much more difficult to describe: Imagine an adequate mathematical description of the shape of a forest (when every leaf and pine needle must be described). Furthermore, land surfaces are seldom homogeneous either horizontally or with depth.

Since a true mathematical description of the ground surface appears out of the question, empirical measurements are necessary to describe the radar return from natural surfaces. The role of theory is to aid in interpreting these measurements and to suggest how they may be extrapolated.

Available Scattering Information. Prior to 1972 the lack of coordinated research programs over the necessary long period resulted in only one really usable set of measurements, that at Ohio State University.^{2,4} Since that time extensive measurements have been made from trucks and helicopters by the University of Kansas,^{6,7} a group in the Netherlands,⁸ and several groups in France.⁹ These measurements concentrated especially on vege-

tation, with the Kansas measurements also including some work on snow and extensive work on sea ice. Most of these measurements were in the 10 to 80° range of incidence angles. Measurements near vertical are scarcer, while well-controlled experiments near grazing are very scarce indeed.

Airborne measurements are necessary to make larger scattering areas accessible. Although airborne programs for special purposes have been legion, curves of scattering coefficient versus angle for a known homogeneous area are scarce. The work at the MIT Radiation Laboratory¹⁰ was early work by Philco Corporation,¹¹ Goodyear Aerospace Corporation,¹² General Precision Laboratory,¹³ and the U.S. Naval Research Laboratory (NRL)¹⁴⁻¹⁶ programs were important early. More recently, the Canada Centre for Remote Sensing (CCRS) has made numerous airborne scatterometer measurements,¹⁷ especially over sea ice. The Environmental Research Institute of Michigan (ERIM),¹⁸ CCRS, the European Space Agency (ESA),¹⁹ and the Jet Propulsion Laboratory (JPL)²⁰ used imaging synthetic aperture radars (SARs) for some scattering measurements, but most were not well calibrated.

Results of most of these measurements are summarized in Ulaby, Moore, and Fung.²¹ More complete summaries of the earlier work and near-grazing studies are in Long.²² Many applications summaries are also in the "Manual of Remote Sensing."²³ Readers requiring more detailed information should consult these books.

12.2 PARAMETERS AFFECTING GROUND RETURN

Radar return depends upon a combination of system parameters and ground parameters:

Radar system parameters [Eqs. (12.1) and (12.2a and b)]

Wavelength

Power

Illuminated area

Direction of illumination (both azimuth and elevation)

Polarization

Ground parameters

Complex permittivity (conductivity and permittivity)

Roughness of surface

Inhomogeneity of subsurface or cover to depth where attenuation reduces wave to negligible amplitude

Different wavelengths are sensitive to different elements on the surface. One of the earliest known and most striking directional effects is the *cardinal-point* effect in return from cities: Radars looking in directions aligned with primary street grids observe stronger regular returns than radars at other angles. When radars are looking at a normal-incidence angle, horizontally polarized waves are reflected better by horizontal wires, rails, etc., than are vertically polarized waves.

If the geometry of two radar targets were the same, the returns would be

stronger from the target with higher complex permittivity because larger currents (displacement or conduction) would be induced in it. Because identical geometries with differing permittivities do not occur in nature, this distinction is not easy to measure. Effective permittivity for ground targets is very strongly influenced by moisture content, since the relative permittivity of liquid water is from about 60 at X band to about 80 at S band and longer wavelengths whereas most dry solids have permittivities less than 8. Attenuation is also strongly influenced by moisture, since wet materials usually have higher conductivity than the same materials dry. Figures 12.3 and 12.4 show the effect of moisture content on properties of plants and of soil. The high permittivity of plants with much moisture means that radar return from crops varies as the plants mature, even when growth is neglected.

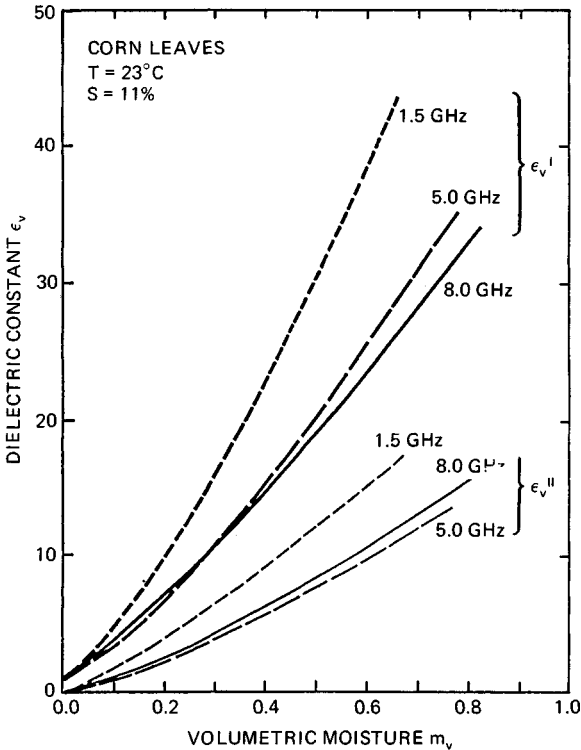


FIG. 12.3 Measured moisture dependence of the dielectric constant of corn leaves at 1.5, 5.0, and 8.0 GHz. S is the salinity of water content in parts per thousand, $\epsilon_v = \epsilon_v' - j\epsilon_v''$ is the complex dielectric constant in Fm^{-1} , and m_v is the volumetric moisture content in $\text{kg}\cdot\text{m}^{-3}$. (After Ulaby, Moore, and Fung.²¹)

The roughness of surfaces (especially natural ones) is difficult to describe mathematically but easy to understand qualitatively. Thus it is easy to see that a freshly plowed field is rougher than the same field after rain and wind have been at work on it. A forest is inherently rougher than either a field or a city. The dif-

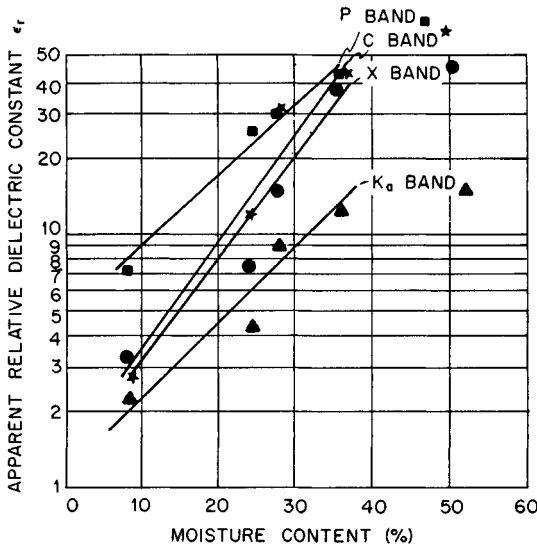


FIG. 12.4 Apparent relative dielectric constant versus moisture content (Richfield silt loam). (After Lundien.²⁴)

ference between the roughness of a city with flat walls interspersed with windowsills, with curbs, cars, and sidewalks, and the roughness of natural areas is harder to see.

Surfaces that are relatively smooth tend to reflect radio waves in accordance with the Fresnel-reflection direction,* and so they give strong backscatter only when the look angle is nearly normal to the surfaces. Rough surfaces, on the other hand, tend to reradiate nearly uniformly in all directions, and so they give relatively strong radar returns in any direction.

The problem of radar scatter is complicated because waves penetrate significant distances into many surfaces and vegetation canopies, and internal reflection and scatter contribute to the return. Measurements of attenuation for field crops^{25,26} and grasses²⁷ show that most of the return is from the upper layers, with some contribution by the soil and lower layers if the vegetation is not very dense. Most of the signal returned from trees is usually from the upper and middle branches when the trees are in leaf,²⁸⁻³² although in winter the surface is a major contributor to the signal.

12.3 THEORETICAL MODELS AND THEIR LIMITATIONS

Descriptions of a Surface. Many theoretical models for radar return from the ground assume a rough boundary surface between air and an infinite homogeneous half space. Some include either vertical or horizontal homogeneities in the ground properties and in vegetative or snow covers.

*Angle of reflection equals angle of incidence.

Surface descriptions suitable for use in mathematical models are necessarily greatly idealized. Few natural grounds are truly homogeneous in composition over very wide areas. Descriptions of their detailed shape must be simplified if they are to be handled analytically, although computers permit the use of true descriptions. Very few surfaces have ever been measured to the precision appropriate for centimeter-wavelength radars; even for these there is no assurance that scattering boundaries do not exist within a skin depth beneath the surface. Surfaces containing vegetation and conglomerate rocks almost completely defy description.

Statistical descriptions of surfaces are used for most theories, since a theory should be representative of some kind of surface class, rather than of a particular surface, and since exact description is so difficult. The statistical descriptions themselves must be oversimplified, however. Many theories assume isotropic statistics, certainly not appropriate for plowed fields or gridded cities. Most theories assume some kind of model involving only two or three parameters (standard deviation, mean slope, correlation distance, etc.), whereas natural (or human-made) surfaces seldom are so simply described. The theories for vegetation and other volume scatterers have more parameters.

Simplified Models. Early radar theories for ground return assumed, as in optics, that many targets could be described by a Lambert-law variation of intensity; that is, the differential scattering coefficient varies as $\cos^2 \theta$, with θ the angle of incidence. This "perfectly rough" assumption was soon found wanting, although it is a fair approximation for the return from many vegetated surfaces over the midrange of angles of incidence.

Clapp¹⁰ described three models involving assemblies of spheres, with different spacings and either with or without a reflecting ground plane. These models yield variations from σ^0 independent of angle through $\sigma^0 \propto \cos \theta$ to $\sigma^0 \propto \cos^2 \theta$. Since the sphere models are highly artificial, only the resulting scatter laws need be considered. Most targets give returns that vary more rapidly over part of the incidence-angle regime than these models, although forests and similar rough targets of some depth sometimes give such slowly varying returns.

Since these rough-surface models usually fail to explain the rise in return near vertical incidence, other simplified models combine Lambert's law and other rough-surface scattering models with specular reflection at vertical incidence, and a smooth curve is drawn between the specular value and the rough-surface prediction.

Specular reflection is defined as reflection from a smooth plane and obeys the Fresnel reflection laws.³³ At normal incidence, the specular-reflection coefficient is therefore

$$\Gamma_R = \frac{\eta_g - \eta_0}{\eta_g + \eta_0}$$

where η_0 , η_g are the intrinsic impedances of air and earth, respectively. The fraction of total incident power specularly reflected from a rough surface is⁵

$$e^{-2(2\pi\sigma_h/\lambda)^2}$$

where σ_h = standard deviation of surface height variations
 λ = wavelength

Since this proportion is down to 13.5 percent when $\sigma_h = \lambda/2\pi$ and to 1.8 percent when $\sigma_h = \lambda/(2\pi\sqrt{2})$, significant specular reflection is seldom found for the centimeter wavelengths usually used for radar. Nevertheless, a simplified model like this is convenient for some purposes.

Observation of reflected sunlight from rippled water, from roads, and from other smooth surfaces leads to the postulation of a facet theory.^{34,35} The only sunlight reaching the observer from smooth surfaces such as water is that from facets for which angle of incidence equals angle of reflection. Thus the observed light may be described by methods of *geometric optics*.

When geometric optics is used to describe radar scatter, the surface of the ground is represented by small flat-plane segments. Radar return is assumed to occur only for facets oriented normal to the radar (normal orientation is required for backscatter so that the reflected wave returns to the source). Thus, if the slope distribution of such facets is known, the fraction normal to a given diverging beam can be established, and from this the return can be obtained. Geometric optics assumes zero wavelength, and so the results of such a theory are wavelength-independent, clearly not in accord with observation.

The facet model for radar return is extremely useful for qualitative discussions, and so modification to make it fit better with observation is appropriate. Two kinds of modification may be used, separately or jointly: considering the actual reradiation pattern of finite-size facets at finite wavelengths³⁶ and considering the effect of wavelength on establishing the effective number of facets.³⁷ Thus the scatter from a facet may actually occur in directions other than that requiring that angle of incidence equal angle of reflection. Figure 12.5 illustrates this. For large facets (compared with wavelength) most of the return occurs almost at normal incidence, whereas for small facets the orientation may be off normal by a considerable amount without great reduction in scatter. As the wavelength is increased, the category of a given facet changes from *large* to *small*; eventually the facet is smaller than a wavelength, and its reradiation pattern shape remains almost isotropic from that point. Many facets that would be separate at, say, a 1-cm wavelength are combined at a 1-m wavelength; the result may be a transition from rough- to smooth-surface behavior. Figure 12.6a shows a number of facets of different sizes contributing to a radar return.

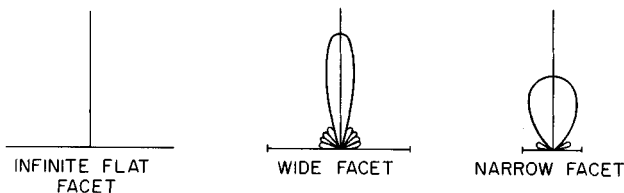


FIG. 12.5 Normal-incidence reradiation patterns of facets.

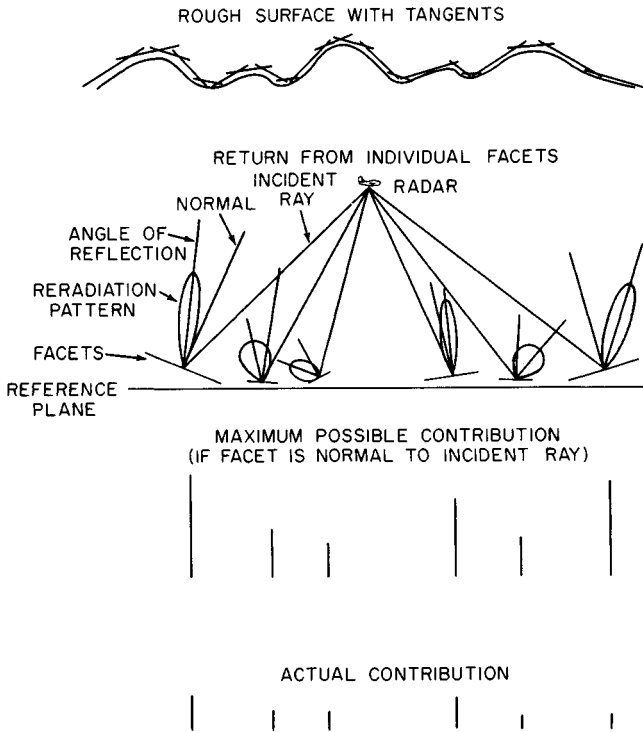


FIG. 12.6a Facet model of a radar return.

Physical Optics Models. Theories based on applications of the Kirchhoff-Huygens principle have been thoroughly developed.^{21,36,38-40} The Kirchhoff approximation is that the current flowing at each point in a locally curved (or rough) surface is the same as would flow in the same surface if it were flat and oriented tangent to the actual surface. This assumption permits construction of scattered fields by assuming that the current over a rough plane surface has the same magnitude as if the surface were smooth, but with phase perturbations set by the differing distances of individual points from the mean plane. For surfaces assumed to be azimuthally isotropic, the usual approach yields integrals of the form

$$\frac{1}{\cos^3 \theta} \int e^{-(2k\sigma_h \cos \theta)^2 [1 - \rho(\xi)]} J_0(2k\xi \cos \theta) \xi d\xi$$

where $\rho(\xi)$ = spatial autocorrelation function of surface heights
 θ = angle with vertical
 σ_h = standard deviation of surface heights
 $k = 2\pi/\lambda$
 J_0 = first-order, first-kind Bessel function

The autocorrelation function of height with distance is seldom known for terrain, although it can be determined on a large scale by analysis of contour maps,⁴¹ and it has been found for some areas by careful contouring at close intervals and subsequent analysis. Because of lack of knowledge of actual autocorrelations, most theory has been developed with artificial functions that are chosen more for their integrability than for their fit with nature; selection among them has been on the basis of which ones yield the best fit between theoretical and experimental scatter curves.

The correlation function first used⁴² was gaussian:

$$\rho(\xi) = e^{-\xi^2/L^2} \quad (12.5)$$

where L is the *correlation length*. Not only is this a function that makes the integral analytically tractable, but it also gives exactly the same results as geometric optics.⁴³ Since it fails, like geometric optics, to explain frequency variation, it cannot be a truly representative correlation function, although it gives a scattering curve that fits several experimental curves near the vertical. The next most frequently used function is the exponential:

$$\rho(\xi) = e^{-|\xi|/L} \quad (12.6)$$

This has some basis in contour-map analysis;⁴¹ the results fit both earth and lunar radar return over a wider range of angles than the gaussian^{41,44} (but sometimes not as well near vertical). Furthermore, it has the merit that it exhibits frequency dependence. Resulting expressions for power (scattering coefficient) variations appear in Table 12.1.

TABLE 12.1 Scattering Coefficient Variation

Correlation coefficient	Power expression	Reference
$e^{-\xi^2/L^2}$	$\frac{K}{\sin \theta} e^{-(L^2/2\sigma_h^2) \tan^2 \theta}$	42
$e^{- \xi /L}$	$\frac{K\theta}{\cos^2 \theta \sin \theta} \left(1 + A \frac{\sin^2 \theta}{\cos^4 \theta}\right)^{-3/2}$	33

Small-Perturbation and Two-Scale Models. Recognition that existing models were inadequate for describing ocean scatter led to recognition that resonance of the signal with small structures on the surface has a powerful influence on the strength of the signal received.^{45,46} Thus a small-perturbation method originally proposed by Rice⁴⁷ became the most popular way to describe ocean scatter. Its application to land scatter was not far behind.

The term *Bragg scatter* is often used to describe the mechanism for the small-perturbation model. The idea comes from the concept illustrated in Fig. 12.6*b*.

A single sinusoidal component of a complex surface is shown with an incoming radar wave at angle of incidence θ . The radar wavelength is λ , and the surface-component wavelength is Λ . When the signal travels an extra distance

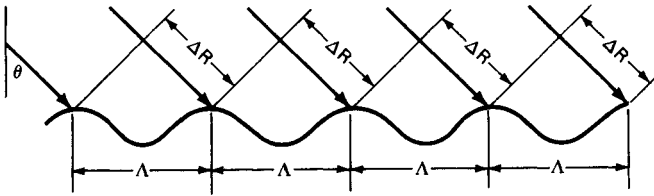


FIG. 12.6b In-phase addition for Bragg scattering; $\Delta R = n\lambda/2$.

$\lambda = 2\Delta R$ between the source and two successive wave crests, the phase difference between the echoes from successive crests is 360° ; so the echo signals all add in phase. If this condition is satisfied for a particular Λ and θ , it fails to be satisfied for others. Thus, this is a resonant selection for a given θ of a particular component of the surface Λ . The strength of the received signal is proportional to the height of this component and to the number of crests illuminated by the radar. If the surface has an underlying curvature, the number of illuminated crests satisfying the resonance criterion may be limited by the length of the essentially flat region; otherwise it is limited by the radar resolution.

The theoretical expression for the scattering coefficient is⁴⁸

$$\sigma_{pq}^0 = 8k^4 \sigma_1^2 \cos^4 \theta |\alpha_{pq}|^2 W(2k \sin \theta, 0) \quad (12.7)$$

where p, q = polarization indices (H or V)

$k = 2\pi/\lambda$ (the radar wavenumber)

$\alpha_{HH} = R_1$ (Fresnel reflection coefficient for horizontal polarization)

$$\alpha_{VV} = (\epsilon_r - 1) \frac{\sin^2 \theta - \epsilon_r (1 + \sin^2 \theta)}{[\epsilon_r \cos \theta + (\epsilon_r - \sin^2 \theta)^{1/2}]^2}$$

where ϵ_r is the relative permittivity $\epsilon' - j\epsilon''$ and $\alpha_{VH} = \alpha_{HV} = 0$.

$W(2k \sin \theta, 0)$ is the *normalized roughness spectrum* (the Fourier transform of the surface autocorrelation function). It may be written as $W(K, 0)$, where K is the wavenumber for the surface. In terms of the wavelength on the surface Λ ,

$$K = 2\pi/\Lambda$$

Thus the component of the surface that satisfies the Bragg resonance condition is

$$\Lambda = \lambda/2 \sin \theta \quad (12.8)$$

The meaning of this is that the most important contributor to a surface return is the component of surface roughness with wavelength Λ . Even though other components may be *much* larger, the Bragg resonance makes this component more important. On the ocean this means that tiny ripples are more important than waves that are meters high; the same applies for land-surface scatter.

As originally developed, this theory was for perturbations to horizontal flat surfaces, but it was soon modified to handle surfaces with large-scale roughness. The large-scale roughness was assumed to cause a *tilting* of the flat surface to which the small-perturbation theory could be applied. The principal problem with this approach is deciding where in the spectrum lies the boundary between the larger components that do the tilting and smaller components that are Bragg-

resonant. Many papers have been written to describe the evolution of this theory; for a complete summary, the reader is referred to Fung's development in Ref. 49.

Other Models. The theory for volume scatter has led to many papers and continues to evolve. For a review of some of the approaches the reader should consult Fung's summary in Ref. 50 and papers by Kong, Lang, Fung, and Tsang. These models have been used reasonably successfully to describe scatter from vegetation,⁵¹ snow,⁵² and sea ice.⁵³ Models of straight vegetation such as wheat in terms of cylinders have had some success.² Corner-reflector effects have been used to describe strong returns from buildings at nonnormal incidence angles.⁵⁴ Other specialized models have been used for particular purposes.

Regardless of the model used and the approach applied to determining the field strength, theoretical work only guides understanding. Actual earth surfaces are too complex to be described adequately in any of the models, and the effects of signals that penetrate the ground and are scattered therein are too little known to permit its evaluation.

12.4 FADING OF GROUND ECHOES

The amplitude of ground echoes received by radars on moving vehicles fluctuates widely because of variations in phase shift for return from different parts of the illuminated area. In fact, even fixed radars frequently observe fluctuations in ground echoes because of motions of vegetation, automobiles, etc.

Regardless of the model used to describe a ground surface, signals are, in fact, returned from different positions not on a plane. As a radar moves past a patch of ground while illuminating it, the look angle changes, and this changes the relative distances to different parts of the surface; the result is that relative phase shift is changed. This is the same kind of relative-phase-shift change with direction that is present for an antenna array and results in the antenna pattern. For ground echo the distance is doubled; so the pattern of an echoing patch of length L has lobes of width $\lambda/2L$. This compares with λ/L for an antenna of the same cross-range length. Because the excitation of the *elements* of the scattering array is random, the scattering pattern in space also is random.

This fading phenomenon is usually described in terms of the doppler shift of the signal. Since different parts of the target are at slightly different angles, the signals from them experience slightly different doppler shifts. The doppler shift, of course, is simply the rate of change of phase due to motion. Thus the total rate of change of phase for a given target is

$$\omega = \omega_c + \omega_{di} = \frac{d\phi_i}{dt} = \frac{d}{dt}(\omega_c t - 2kR_i) \quad (12.9)$$

where ω_c = carrier angular frequency

ω_{di} = doppler angular frequency for i th target

ϕ_i = phase for i th target

R_i = range from radar to i th target

The doppler shift can be expressed in terms of the velocity vector \mathbf{v} as

$$\omega_{di} = -2k \frac{dR_i}{dt} = -2k \mathbf{v} \cdot \frac{\mathbf{R}_i}{R_i} = -2k v \cos(\mathbf{v}, \mathbf{R}_i) \quad (12.10)$$

Hence the total field is given by

$$E = \sum_i A_i \exp \left\{ j \left[\omega_c t - \int_0^t 2k \mathbf{v} \cdot \frac{\mathbf{R}_i}{R_i} dt - 2kR_{i0} \right] \right\} \quad (12.11)$$

where A_i is the field amplitude of the i th scatterer and R_{i0} is the range at time zero.

The only reason the scalar product is different for different scatterers is the different angle between the velocity vector and the direction to the scatterer. This results in a different doppler frequency for each scatterer. If we assume the locations to be random, as most theories do, the received signal is the same as one coming from a set of oscillators with random phases and unrelated frequencies. This same model of a group of randomly phased, different-frequency oscillators is used to describe noise; *thus the statistics of the fading signal and the statistics of random noise are the same.*

This means that the envelope of the received signal is a random variable with its amplitude described by a Rayleigh distribution. Such distributions have been measured for many ground-target echoes.¹⁵ Although the actual distributions vary widely, no better description can be given for relatively homogeneous targets.

When a target is dominated by one large echo (such as a metal roof oriented to give a strong return), the distribution is better described by that for a sine wave in noise. If the large echo is considerably stronger than the mean of the remaining contributors to the return, this approaches a normal distribution about the value for the large echo. In practice, the distribution from large targets may be more complicated than either of the simple models described.

For reference, the two distributions are given:⁵⁵

$$p(v)dv = \frac{v}{\psi_0} e^{-v^2/2\psi_0} dv \quad (\text{Rayleigh})$$

$$p(v)dv = \frac{v}{\psi_0^{1/2}} e^{-(v^2 + a^2)/2\psi_0} I_0\left(\frac{av}{\psi_0}\right) dv \quad (\text{sine wave + noise})$$

where v = envelope voltage

ψ_0 = mean square voltage

a = sine-wave peak voltage

$I_0(x)$ = Bessel function, first kind, zero order, imaginary argument

Fading-Rate Computations. Doppler frequency calculation is the easiest way to find fading rates. To compute the signal amplitude returned with a particular range of doppler shifts, all signals having such shifts must be summed. This requires knowledge of the contours of constant doppler shift (isodops) on the scattering surface. These contours must be established for each particular geometric arrangement. A simple example is presented here: horizontal motion over a plane earth. This is typical of an aircraft in ordinary cruising flight.

Consider travel in the y direction, with z vertical, and the altitude (fixed) $z = h$. Then

$$\mathbf{v} = \mathbf{1}_y v$$

$$\mathbf{R} = \mathbf{1}_x x + \mathbf{1}_y y - \mathbf{1}_z h$$

where $(\mathbf{1}_x, \mathbf{1}_y, \mathbf{1}_z)$ are unit vectors. Hence

$$v_r = \mathbf{v} \cdot \frac{\mathbf{R}}{R} = \frac{vy}{\sqrt{x^2 + y^2 + h^2}}$$

where v_r is the relative speed. Curves of constant relative speed are also curves of constant doppler shift. The equation of such a curve is

$$x^2 - y^2 \frac{v^2 - v_r^2}{v_r^2} + h^2 = 0$$

This is a hyperbola. The limiting curve for zero relative speed is a straight line perpendicular to the velocity vector. Figure 12.7 shows such a set of constant-doppler-shift contours.

The spectrum of fading can be calculated by a slight rearrangement of the radar equation (12.1). Thus, if $W_r(f_d)$ is the power received between frequencies f_d and $f_d + df_d$, the radar equation becomes

$$W_r(f_d)df_d = \frac{1}{(4\pi)^2} \int_{\text{Illuminated area between } f_d \text{ and } f_d + df_d} \frac{P_t G_t A_r \sigma^0 dA}{R^4} = \frac{df_d}{(4\pi)^2} \int \frac{P_t G_t A_r \sigma^0}{R^4} \left(-\frac{dA}{df_d} \right) \quad (12.12)$$

This is an integral in which the area element between f_d and $f_d + df_d$ is expressed in terms of coordinates along and normal to the isodops. Such coordinates must be established for each particular case.

Figure 12.8 shows the geometry for horizontal travel. The coordinate σ is along the isodop, and η is normal to it. We can express Eq. (12.12) in terms of these coordinates as

$$W_r f_d = \frac{d\eta}{df_d} \left[\frac{\lambda^2}{(4\pi)^3} \right] \int_{\text{strip}} \left[\frac{P_t G^2 \sigma^0 d\xi}{R^4} \right] \quad (12.13)$$

Note that P_t , the transmitted power, is nonzero in the integral only for the time it illuminates the ground. In pulse radars, only that part of the ground area providing signals back to the radar at a particular time can be considered to have finite P_t , and so the range of frequencies that can be present is limited by the pulse, as well as by the antennas and the maximum velocity.

Another example is shown in Fig. 12.9. This is the small illuminated area for a narrow-beam, short-pulse system. Here we can make linear approximations with-

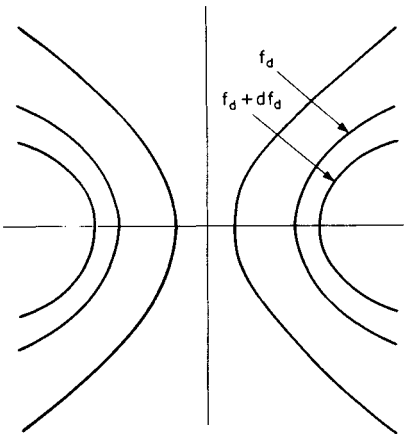


FIG. 12.7 Contours of constant doppler frequency shift on a plane earth due to horizontal motion.

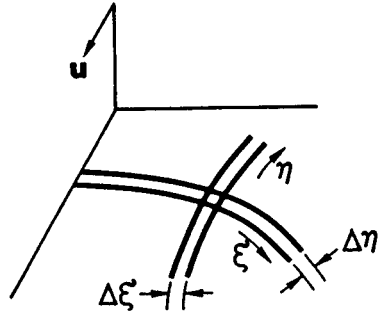


FIG. 12.8 Geometry of complex fading calculations. (From Ulaby, Moore, and Fung.²¹)

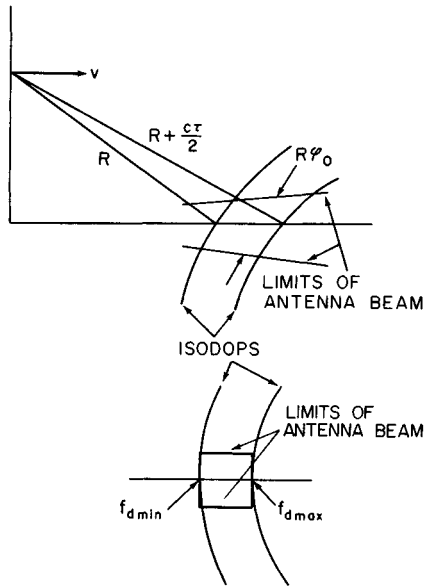


FIG. 12.9 Geometry of doppler-shift calculations for an airborne search radar.

out too much error. A pulse of length τ is transmitted from an antenna of beamwidth ϕ_0 . For the simple illustration given here, we assume the pulse to be transmitted directly ahead of the horizontally moving vehicle. We may simplify the problem by assuming a rectangular illuminated area, $R\phi_0$ by $c\tau/(2 \sin \theta)$. Furthermore, the curvature of the isodops may be neglected, and so the doppler fre-

quency is assumed to be the same for all maximum-range points and the same for all minimum-range points. With this assumption,

$$f_{d\max} = \frac{2v}{\lambda} \sin \theta_{\max}$$

$$f_{d\min} = \frac{2v}{\lambda} \sin \theta_{\min}$$

Thus the total width of the doppler spectrum is

$$\Delta f_d = \frac{2v}{\lambda} (\sin \theta_{\max} - \sin \theta_{\min})$$

For short pulses and angles away from vertical, this is

$$\Delta f_d \approx \frac{2v}{\lambda} \Delta \theta \cos \theta$$

In terms of pulse length, it becomes

$$\Delta f_d = \frac{vc\tau \cos^3 \theta}{2h\lambda \sin \theta} \quad (12.14)$$

If the angular difference across the illuminated rectangle is small enough so that σ^0 is essentially constant, the doppler spectrum is a rectangle from f_{\min} to f_{\max} .

In practice, antenna beams are not rectangular. The result is that the doppler spectrum for a side-looking radar like that of the example is not rectangular but rather has the shape of the antenna along-track pattern. Thus, if the antenna pattern in the along-track direction is $G = G(\beta)$, with β the angle off the beam center, we can express β in terms of the doppler frequency f_d as

$$\beta = f_d \lambda / 2v$$

and the spectrum is

$$W(f_d) = \frac{\lambda^3 P_r \sigma^0 r_x}{2(4\pi)^3 R^3} G^2 \left[\frac{\lambda f_d}{2v} \right]$$

where r_x is the horizontal resolution in the range direction. Of course, the half-power beamwidth may be used as an approximation, resulting in the bandwidth given by Eq. (12.13).

Effect of Detection. The effect of detecting narrowband noise has been treated extensively in the literature. Here it is necessary only to show the postdetection spectrum of the preceding example and to consider the number of independently fading samples per second. Figure 12.10 shows the spectrum before and after detection. If square-law detection is assumed, the post-detection spectrum is the self-convolution of the predetection spectrum. Only the part that passes the low-pass filters in a detector is shown in the figure. The rectangular *RF spectrum* has become a triangular *video spectrum*.

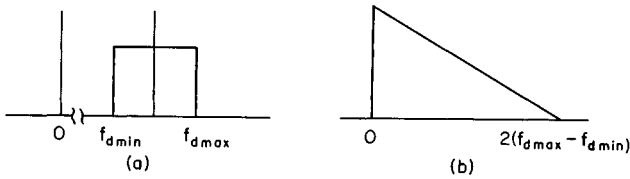


FIG. 12.10 Spectrum of fading from a homogeneous small patch (a) before and (b) after detection.

This spectrum describes the fading of the detector output for a CW radar. For a pulse radar, the spectrum is sampled by the PRF (pulse repetition frequency). If the PRF is high enough so that the entire spectrum can be reproduced (the PRF is higher than the Nyquist frequency, $2\Delta f_d$), the diagram indicated is that of the spectrum of the samples of a received pulse at a given range. Figure 12.11 shows a series of actual pulses, followed by a series of samples at range R_1 . The spectrum of Fig. 12.10 is the spectrum of the envelope of samples at R_1 (after low-pass filtering). The spectrum of fading at a different range (or vertical angle) is different, in accord with Eq. (12.13).

For many purposes, the number of *independent* samples is important, since these may be treated by using the elementary statistics of uncorrelated samples. For continuous integration, the effective number of independent samples is⁵⁵

$$N = \frac{\bar{P}_e T}{2 \int_0^T \left[1 - \frac{x}{T}\right] R_{sf}(x) dx} \quad (12.15)$$

where \bar{P}_e is the mean envelope power, T is the integration (averaging) time, and $R_{sf}(t)$ is the autocovariance function for the detected voltage. For many practical purposes, if N is large, it may be approximated by

$$N \approx BT \quad (12.16)$$

where B is the effective IF bandwidth. For the effect of short integration time, see Ref. 56.

Fading samples can, of course, also be independent because motion of the vehicle causes the beam to illuminate a different patch of ground. Thus, in a particular case, the independent-sample rate may be determined either by the motion of the illuminated patch over the ground or by the doppler effect, or by some combination of the two.

The number of independent samples determines the way in which the Rayleigh or other distributions may be applied. Thus, if 100 pulses give only 10 independent samples, the variance of the mean obtained by integrating these pulses is much greater than would be true if all 100 pulses were independent.

Doppler-based systems, such as doppler navigators and synthetic aperture radar systems, depend on the predetection spectrum for their operation, since they are coherent and do not use ordinary detection.

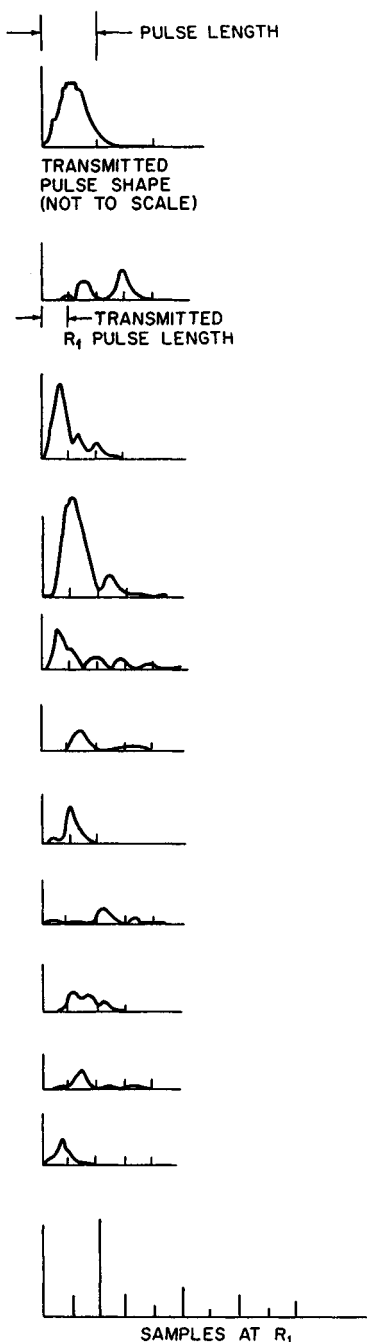


FIG. 12.11 Fading for successive pulses of a radar with ground target.

Moving-Target Surfaces. Sometimes clutter has internal motion. This can occur when fixed radars are used to observe movement of the sea and the land. On land, clutter motion is usually due to moving vegetation, although moving animals and machines create similar effects. The radar return from an assembly of scatterers like those of Fig. 12.8 can change because of motion of the individual scatterers just as it changes because of motion of the radar. Thus, if each scatterer is a tree, the waving of the trees as the wind blows causes relative phase shifts between the separate scatterers; the result is fading. For a fixed radar, this may be the only fading observed, except for very slow fading due to changes in refraction. For a moving radar, this motion of the target changes the relative velocities between target element and radar, so that the spectrum is different from that for a fixed surface. The width of the spectrum due to vehicle motion determines the ability of the radar to detect this target motion.

12.5 MEASUREMENT TECHNIQUES FOR GROUND RETURN

Special-purpose instrumentation radars and modified standard radars may be used to determine the ground return. Since the ground return is almost invariably due to scattering, these systems are termed *scatterometers*. Such systems may use CW signals with or without doppler processing, but they may also use both pulse and FM techniques. Scatterometers capable of measuring response over a wide range of frequencies are called *spectrometers*.⁵⁷ Various antenna patterns from pencil beams to fan beams may be used.

CW and FM-CW Systems. The simplest scatterometer uses a stationary CW radar. Such systems are not very flexible, but they are discussed here in some detail to illustrate calibration techniques that also apply to the more complex systems.

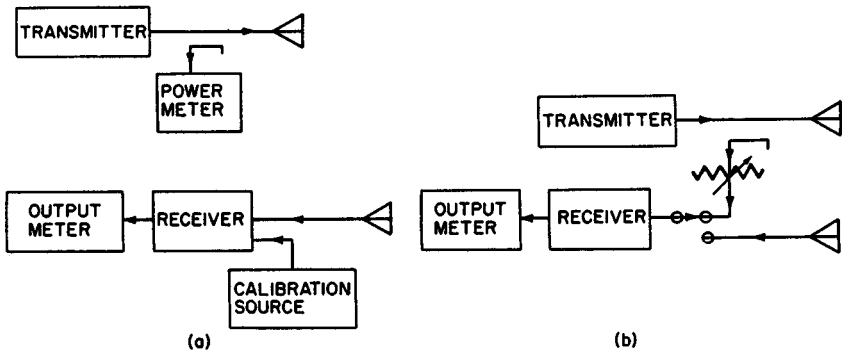


FIG. 12.12 CW-scatterometer-system block diagram. (a) Separate transmitter and receiver calibration. (b) Calibration of the ratio of received to transmitted power.

The CW scatterometer is shown in block form in Fig. 12.12. To evaluate σ^0 the ratio of transmitted to received power is required. The system in Fig. 12.12a measures transmitter power and receiver sensitivity separately. The transmitter feeds an antenna through a directional coupler so that a portion of the energy may be fed to a power meter. The receiver operates from a separate antenna (electrically isolated). The output of the receiver is detected, averaged, and displayed on a meter, oscilloscope, or other display or recorder. Its sensitivity must be checked by use of a calibration source. The calibrated signal may be fed through the receiver at a time when the transmitter is off. Figure 12.12b shows a similar arrangement in which the signal from the transmitter is attenuated a known amount and used to check the receiver. By comparing the output from the attenuated transmitter signal with that received from the ground, the scattering cross section may be determined without actually knowing the transmitted power and the receiver gain.

The calibrations shown in Fig. 12.12 are incomplete without knowledge of the antenna patterns and absolute gains. Since accurate gain measurements are difficult, absolute calibrations may be made by comparing received signals (with proper relative calibration) from the target being measured and from a *standard target*. Standard targets may be metal spheres, Luneburg-lens reflectors, metal plates, corner reflectors, or active radar calibrators (ARCs—actually repeaters).⁵⁸ Of the passive calibrators, the Luneburg-lens reflector is best, since it has a large cross section for its volume and has a very wide pattern so that alignment is not critical. Luneburg-lens reflectors are used for making strong radar targets of small vessels, and they may be obtained from companies that supply that market. For discussion of the relative merits of different passive calibration targets, see Ulaby, Moore, and Fung.⁵⁹

The ideal receiver would respond linearly to its input, so that a single calibration at one input level would suffice for all levels. The usual receiver, however, has some nonlinearities due to detector properties and to saturation of its amplifiers by large signals. Figure 12.13 shows a typical input-output curve for a receiver. Two equal increments in input signal (ΔI), as shown, produce different increments in output because of the nonlinearity of this curve. For this reason, receiver calibration must be performed over a range of input levels, and the nonlinearities must be compensated for in the data processing.

CW scatterometers depend on antenna beams to discriminate different angles

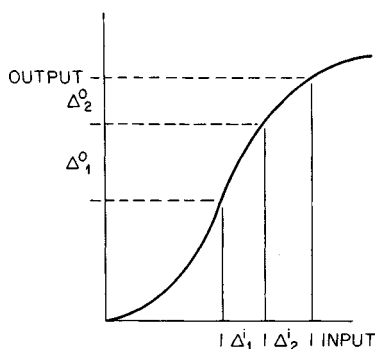


FIG. 12.13 Typical receiver input-output curve. Illustrated is the effect of non-linearity.

of incidence and different targets. Usually assumptions are made that the antenna pattern has constant gain within the actual 3 dB points and zero gain outside, but this clearly is not an accurate description. If large targets appear in the locations illuminated by the side of the main lobe or the minor lobes, their signals may contribute so much to the return that it is significantly changed. Since this changed signal is charged to the direction of the major lobe by the data reduction process, the resulting value for σ^0 is in error. Responses at vertical incidence frequently cause trouble, for vertical-incidence signals are usually fairly strong. Thus the antenna pattern must be accurately known and taken into account in the data analysis. A

pattern with strong minor lobes may be simply inadmissible.

The scattering coefficient is determined by applying

$$P_r = \frac{P_t \lambda^2}{(4\pi)^3} \int_{\text{Illuminated area}} \frac{G_i^2 \sigma^0 dA}{R^4}$$

The integration is over whatever area is illuminated significantly, including the regions hit by the minor lobes. The usual assumption is that σ^0 is constant over the illuminated area, so that

$$P_r = \frac{P_t \lambda^2 \sigma^0}{(4\pi)^3} \int_{\text{Illuminated area}} \frac{G_i^2 dA}{R^4} \quad (12.17)$$

This assumption would be true only if the antenna confined the radiated energy to a very small spread of angles and to a fairly homogeneous region. The resulting expression is

$$\sigma^0 = \frac{(4\pi)^3 P_r}{P_t \lambda^2 \int_{\text{Illuminated area}} (G_i^2 / R^4) dA} \quad (12.18)$$

Note that only the ratio of transmitted to received power is required, and so the technique of Fig. 12.12b is justified. Sometimes R , G_i , or both are assumed constant over the illuminated area, but such an approximation to Eq. (12.18) should be attempted only after checking its validity for a particular problem.

If the result of applying the technique of Eq. (12.18) to a set of measurements indicates that σ^0 probably did vary across the significantly illuminated area, this variation may be used as a first approximation to determine a function $f(\theta)$ describing the θ variation of σ^0 , and a next-order approximation then becomes

$$\sigma^0 = \frac{(4\pi)^3 P_r}{P_t \lambda^2 \int_{\text{Illuminated area}} [f(\theta) G_t^2 / R^4] dA} \quad (12.19)$$

Proper scattering measurements demand an accurate and complete measurement of antenna gain G_t . This can be a very time-consuming and expensive process, particularly when the antenna is mounted on an aircraft or other metallic object. Nevertheless, complete patterns are a must for good scatter measurements.

Range-Measuring Systems. Radar's ability to separate returns from different ranges can be used advantageously along with directive antenna beams to simplify the scattering measurements. Most ranging scatterometers use either pulse modulation or FM, although more exotic modulations could also be used. The discussion here treats pulse systems, but since all other range-measuring systems can be reduced to equivalent pulse systems most results are general.

Figure 12.14 shows the way in which pulse measurement of range is used. Figure 12.14a shows a circular pencil beam. At angles near grazing, the illuminated patch set by the circular antenna pattern becomes rather long (the patch is an ellipse), and use of the pulse length to confine illumination to a part of the patch is helpful. Many systems that use beamwidth to set the measured area near vertical use range resolution for angles beyond, say, 60° .

Figure 12.14b shows an antenna pattern that takes better advantage of the possibilities of range measurement. A fan beam is used to illuminate a narrow strip along the ground, and the range resolution permits separating the returns from different angles by the time they return. This technique is especially effective at angles away from the vertical, for the resolution near the vertical is much poorer than near grazing. The simple approach assumes a constant gain across the beam and zero elsewhere:

$$G_t = 0 \quad \phi_a < 2 f_0/2 \quad \text{or} \quad \phi_a > f_0/2$$

$$G_t = G_o \quad -\phi_0/2 < \phi_a < \phi_0/2$$

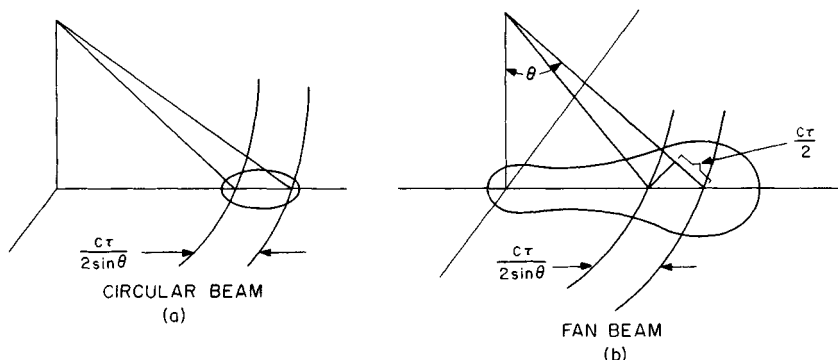


FIG. 12.14 Range resolution applied to scatterometry. (a) Improving one dimension of a circular-beam illumination pattern. (b) Use with a fan beam.

where ϕ_0 = beamwidth

ϕ_a = transverse angle with respect to antenna axis

With the further assumption that σ^0 is essentially constant and that the difference in range across a resolution element is negligible, the expression for σ^0 becomes

$$\sigma^0 = \frac{P_r (4\pi)^3 R^3 \sin \theta}{P_t \lambda^2 G_0 \phi_0 r_R}$$

where r_R is the short-range resolution.

Janza has reported details of calibration problems with a range-measuring pulsed radar scatterometer.^{60,61}

CW-Doppler Scatterometers. A convenient way to measure the scattering coefficient at many angles simultaneously is with a CW system in which the relative velocities corresponding to different angles are separated by separating their doppler frequencies. The use of a fan beam with such a system permits the simultaneous measurement of scattering coefficients at points ahead of and behind the aircraft carrying the radar. Figure 12.15 shows this. The pattern of the antenna illumination on the ground is shown intersected by two isodops (lines of constant doppler frequency), with the width of the spectrum between them shown on the diagram. The distance between them can be seen to be

$$\Delta \rho = R(\sin \theta_2 - \sin \theta_1)$$

and

$$\Delta f_d = \frac{2v}{\lambda}(\sin \theta_2 - \sin \theta_1)$$

Thus the width of the element on the ground is related to the doppler frequency bandwidth by

$$\Delta \rho = \frac{R\lambda}{2v}(\Delta f_d)$$

Where this technique is applied to the radar equation and the following are assumed:

1. σ^0 constant in the illuminated area

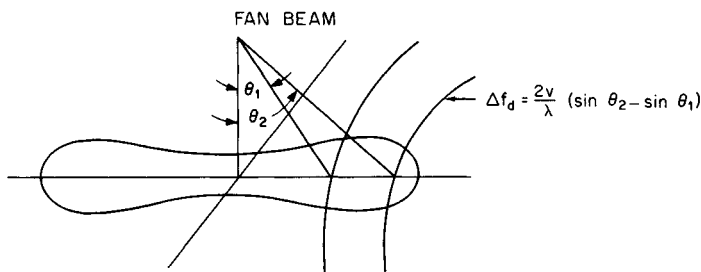


FIG. 12.15 Resolution in a fan-beam CW-doppler scatterometer.

2. Antenna gain constant over its beamwidth and zero elsewhere
3. Range variation across the small illuminated area negligible

$$P_r = \frac{P_t \lambda^2}{(4\pi)^3} \int \frac{G_t^2 \sigma^0 dA}{R^4} = \frac{P_t \lambda^4 \sigma^0 G_0^2 \psi_0 \Delta f_d}{2\nu R^2} \quad (12.21)$$

and so

$$\sigma^0 = \frac{P_r}{P_t} \frac{2\nu R^2}{\lambda^4 G_0^2 \psi_0 \Delta f_d} \quad (12.22)$$

Doppler scatterometers need not use fore-and-aft beams. The Seasat⁶² and N-SCATT⁶³ spaceborne doppler scatterometers were designed with beams pointed (squinted) ahead and behind the normal to the ground track.

Independent Samples Required for Measurement Accuracy. The Rayleigh distribution describes the fading signal fairly well. If we assume a Rayleigh distribution of fading, the number of independent samples required for a given accuracy is shown in Fig. 12.16. The *range* defined in this figure is the range of mean values lying between 5 and 95 percent points on the distribution. This accuracy range is independent of any accuracy problems associated with calibration and knowledge of the antenna pattern.

The precision of the measurement depends upon the number of independent samples, not on the total number of samples. The number of independent samples can be found from Eq. (12.15) or Eq. (12.16) after suitable analysis. This analysis assumes that only doppler fading contributes to independence but motion from one cell to another also adds independent samples. Thus, the total number of such samples is approximately the product of the number calculated from Eq. (12.13) and the number of ground cells averaged. Figure 12.17 shows some examples of the effect of the angle of incidence on the number of independent samples for a horizontally traveling scatterometer with a forward-pointed beam.

Study of the results obtained in this type of analysis indicates that, in regions where the scattering coefficient does not change rapidly with angle, the widest possible angular width (obtained by a longer pulse or a wider filter for a CW-doppler system) results in the maximum number of independent samples for a given distance traveled along the ground.

Near-Vertical Problem Most published radar return data purporting to include vertical incidence gives vertical-incidence scattering coefficients that are too small. This is a consequence of a fundamental problem in measuring near the vertical with a finite beamwidth or pulse length. Near-vertical radar returns from most targets drop off rapidly as the angle with the vertical is increased. Thus the

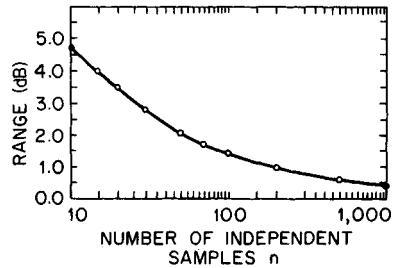


FIG. 12.16 Accuracy of averages for fading signals.

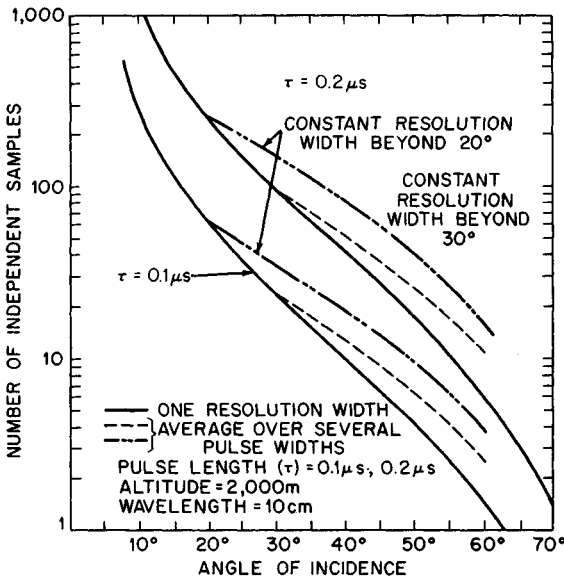


FIG. 12.17 Examples of the variation with angle of incidence of the number of independent samples for a scatterometer.

measuring beamwidth or pulse width usually encompasses signals from regions having values for σ^0 many decibels apart. Since the scattering coefficient varies much more rapidly near the vertical than at angles beyond 10 or 20° from the vertical, the problem is much more severe at the vertical. Furthermore, the problem is complicated at the vertical by the fact that the angular scale terminates there, so that a beam centered at the vertical illuminates weaker targets (σ^0) on both sides of its pattern, whereas a beam away from the vertical illuminates stronger signals on one side and weaker signals on the other.

Figure 12.18 shows what happens for a steeply descending curve of σ^0 versus θ . The radar return integral from Eq. (12.1) is a convolution integral; the figure shows the convolution of the beam pattern with the σ^0 curve. Clearly the average at the vertical is lower than it should be to indicate properly the variation of σ^0 near the vertical.

Figure 12.19 shows an example⁶⁴ based on the theoretical scattering coefficient for the sea derived from the spectra reported by the Stereo Wave Observation Project.⁶⁵ The effect of different beamwidths is clearly shown.

With a pulse or other range-measuring system, reported values are always in error because, as indicated above, it is almost impossible to resolve a narrow range of angles near the vertical.

Ground and Helicopter Scatterometers and Spectrometers. Many ground scattering measurements have been made with systems mounted on boom trucks and helicopters. Most of these are FM-CW systems^{66,67} that use wide bandwidth to obtain extra independent samples rather than for fine resolution. Some use very wide bandwidth to obtain fine range resolution to locate sources of scattering.⁶⁸ Most have multiple-polarization capability, and some are capable of polarimetry because the phase of two received signals with orthogonal polarization can be measured.

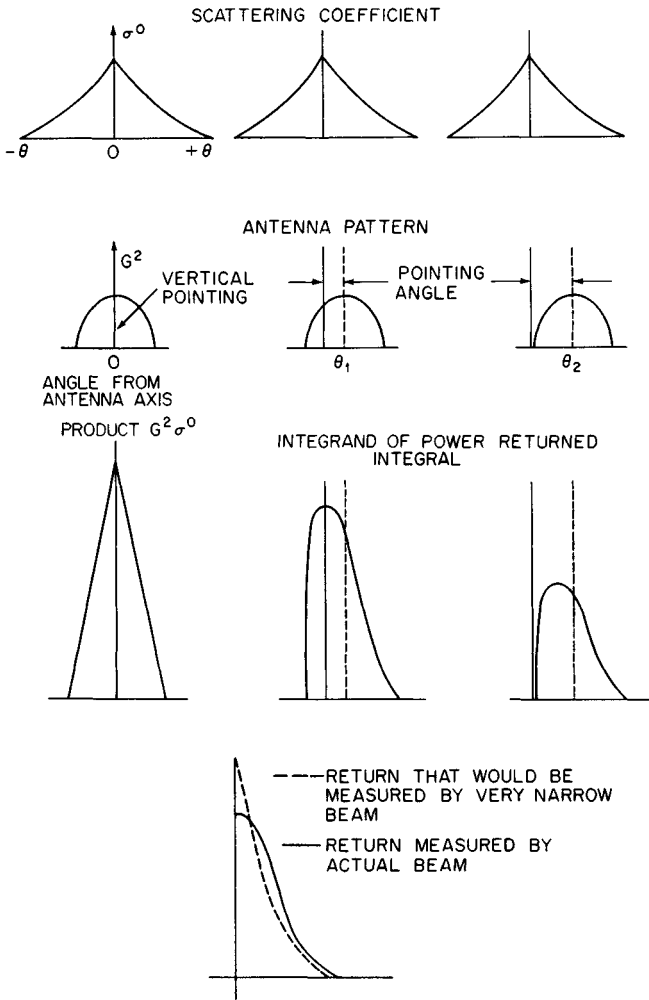


FIG. 12.18 How finite beamwidth causes a near-vertical error in measuring the scattering coefficient.

The basic elements of an FM-CW scatterometer are shown in Fig. 12.20. The swept oscillator must produce a linear sweep; this is easy with yttrium-iron-garnet (YIG)-tuned oscillators but requires linearizing circuits if tuning uses a varactor. If dual antennas are used (as shown), the overlap of the beams must be considered.⁶⁹ Single-antenna systems are sometimes used, with a circulator isolating transmitter and receiver; their performance is somewhat poorer than that of dual-antenna systems because of internal reflections and leakage through the circulator.

Two versions of the control and data-handling part of an FM-CW scatterometer are shown in Figs. 12.21 and 12.22. Figure 12.21 shows the common range-tracking scatterometer. This system can be used to measure

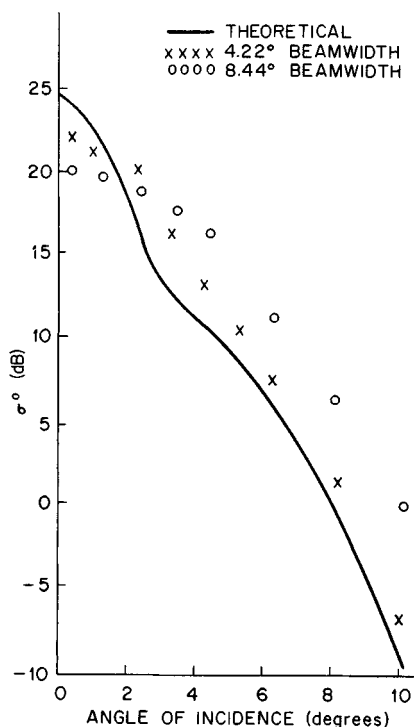


FIG. 12.19 Effect of antenna beamwidth on the measured scattering coefficient as a function of angle of incidence.

surface scattering coefficients when the distance between radar and target is changing, such as with a fixed radar observing the sea or a radar on a helicopter. If the scatterometer is mounted on a boom truck, the range tracker is not needed; but it is convenient because the range changes as the angle of incidence is changed. Figure 12.22 shows the kind of system that may be used to measure scattering from within a volume. By determining the spectrum of the return, the user can establish the scattering from different ranges. This system has been used in determining the sources of scatter in vegetation²⁵⁻²⁷ and snow.

Ultrasonic waves in water can be used to simulate electromagnetic waves in air.⁷⁰⁻⁷² Because of the difference in velocity of propagation an acoustic frequency of 1 MHz corresponds with a wavelength of 1.5 mm. Such a wavelength is of a convenient size for many modeling measurements, and, of course, equipment in the 1-MHz region is in many ways easier to operate than equipment in the microwave region; certainly it is much easier to operate and less expensive than microwave equipment operating at a 1.5-mm wavelength.

Acoustic plane waves and electro-

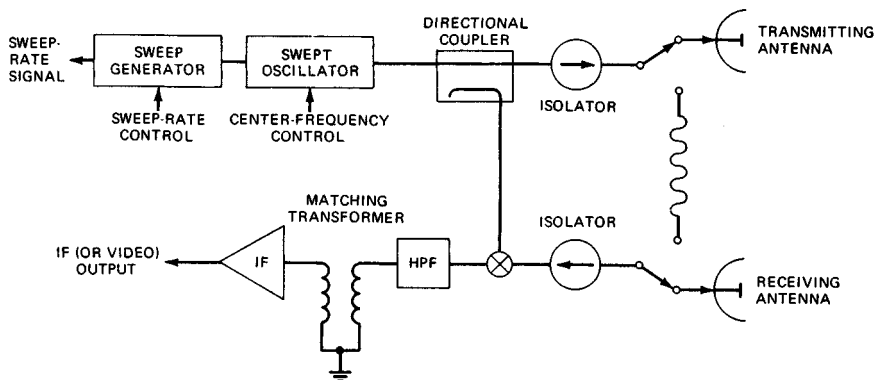


FIG. 12.20 Basic block diagram of an FM-CW scatterometer RF section.

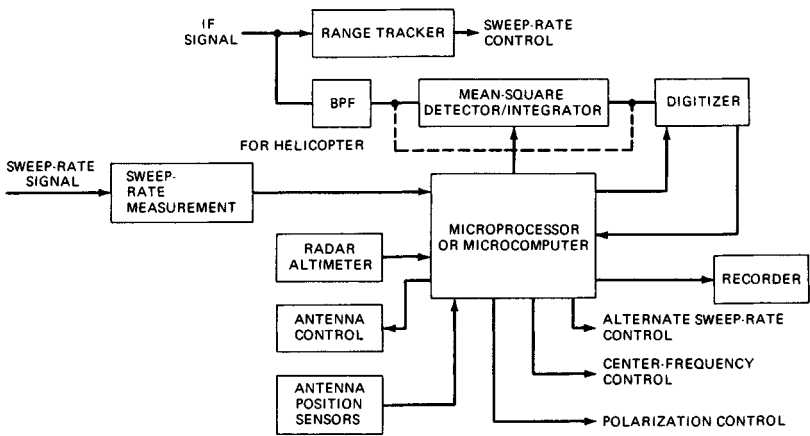


FIG. 12.21 Basic block diagram of an FM-CW range-tracking scatterometer: control and data-handling system.

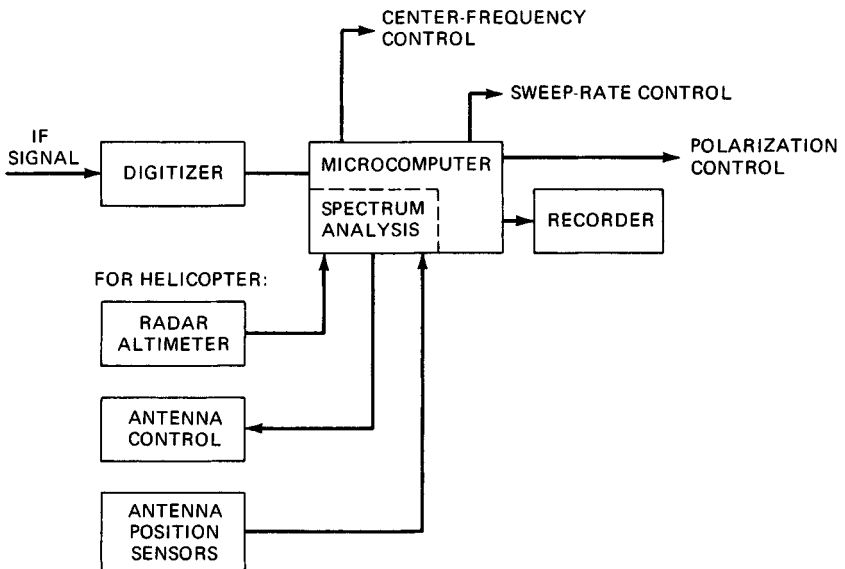


FIG. 12.22 Basic block diagram of an FM-CW range-discriminating scatterometer: control and data-handling system.

magnetic plane waves satisfy the same boundary conditions. When the scattering surfaces are not plane and when angles of incidence are rather oblique, the analogy between acoustic and electromagnetic waves is less valid.

Scattering Coefficients from Images. Radar images produced by real or synthetic aperture radars can be used for scattering coefficient measurement. Unfortunately, most such systems are uncalibrated; so the results are somewhat dubious, even on a relative basis when images are produced on different days. Relative calibration has been introduced into some systems.^{12,18,20,73-75} Absolute calibration, which also serves as relative calibration in some cases, can be achieved by using strong reference targets, with the ARC repeaters especially suitable.⁷⁶ Another approach that has been used is to measure scattering from reference areas with a ground-based or helicopter system that is well calibrated and to compare the images to these measured values.^{73,77}

Bistatic Measurements. Measurements of ground return when the receiver and transmitter are separated are comparatively rare. These measurements are very difficult to make from aircraft because it is necessary that both transmitter and receiver antennas look at the same ground point at the same time and that the signal be correlated with known antenna look angles. Furthermore, it is difficult to know the polarization, and the exact size and shape of the common area illuminated by the antenna beams are sometimes difficult to determine. For this reason, few bistatic measurements from aircraft have been reported in the literature.⁷⁸

Laboratory bistatic measurements have been made by both the Waterways Experiment Station²⁴ and Ohio State University^{2,4} groups using electromagnetic waves and by the University of Kansas⁷¹ group using acoustic waves. Bistatic measurements of laser radiation have been made at Bell Telephone Laboratories,⁷⁹ and C-band measurements of buildings at the University of Kansas.⁸⁰

Because of the antenna orientation problems, most electromagnetic bistatic measurements are only for forward scatter; that is, the receiver, transmitter, and target all lie in the same vertical plane. The acoustic measurements and optical measurements are easier to make over a wide range of angles and have been made with a fixed incidence angle and scatter directions covering the entire hemisphere.

Bistatic measurements call for additional calibration complications when made outside the laboratory because an absolute reference for both transmitter power and receiver sensitivity must be used. In the laboratory, however, it is possible to use techniques similar to those for monostatic measurements.

12.6 GENERAL MODELS FOR SCATTERING COEFFICIENT (CLUTTER MODELS)

Scatter measurements made during the 1970s allowed generation of models for average backscatter from large areas. In particular, these included measurements with the Skylab radiometer-scatterometer RADSCAT⁸³ and with truck-mounted microwave active spectrometers (MAS)⁸¹ by the University of Kansas. Two different models were developed based on the same data, one a linear model and one a more complicated formulation. Here we present only the linear model.

These models are for *averages*, and the models do not include variations about the average. However, analysis of Shuttle Imaging Radar-B (SIR-B) data permits some estimates to be made of the variability to be expected for different sizes of illuminated footprint.

The general characteristics of radar backscatter over the range of angles of incidence have been known for decades. Figure 12.23 shows these. For like-polarized waves, one can break scatter into three angular regimes: near-vertical (the *quasi-specular region*), intermediate angles from 15 to about 80° (the *plateau region*), and near-grazing (the *shadow region*). Cross-polarized scatter does not have separate quasi-specular and plateau regions (the plateau extends to vertical), and too little is known to establish whether a shadow region exists.

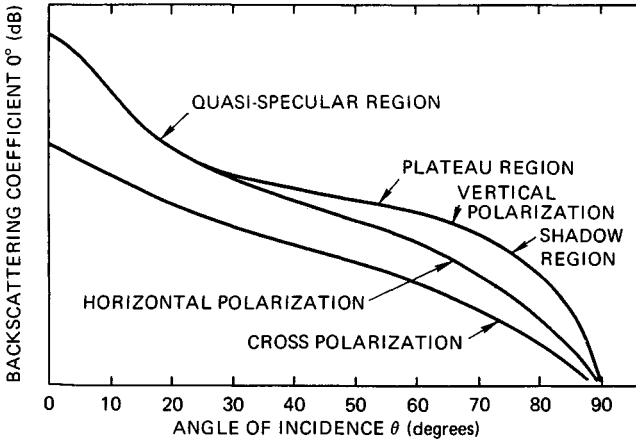


FIG. 12.23 General characteristics of scattering coefficient variation with angle of incidence. (From Ulaby, Moore, and Fung.²¹)

For nearly every type of terrain, the measured data fits closely to the form

$$\sigma^0 = A_i e^{-\theta/\theta_i} \quad (12.23a)$$

$$\text{or} \quad \sigma_{\text{dB}}^0 = 10 \log A_i - 4.3434(\theta/\theta_i) \quad (12.23b)$$

where A_i and θ_i differ for the near-vertical and midrange regions. Figure 12.24 shows an example of this variation. No theory gives exactly this result, but nearly all measurements fit such a model closely, and the model approximates most theoretical curves well over the relevant regions. This simple result means that simple clutter models may be developed and used although more complex models may be necessary for some remote-sensing applications.

The basis for the linear model⁸² is a combination of the Skylab results over North America⁸³ and those from Kansas cropland measurements over three complete seasons with the microwave active spectrometer (MAS).⁸⁴ The 13.9-GHz Skylab RADSCAT had a ground footprint of from a 10-km circle at vertical to an ellipse of 20 by 30 km at 50°. The MAS had footprints at 50° ranging from 5.5 by 8.5 m at 1.1 GHz to 1.4 by 2.1 m at 17 GHz, but millions of measurements were averaged for the model. Because the Skylab data was at only one frequency and the responses for the two experiments were essentially the same at that

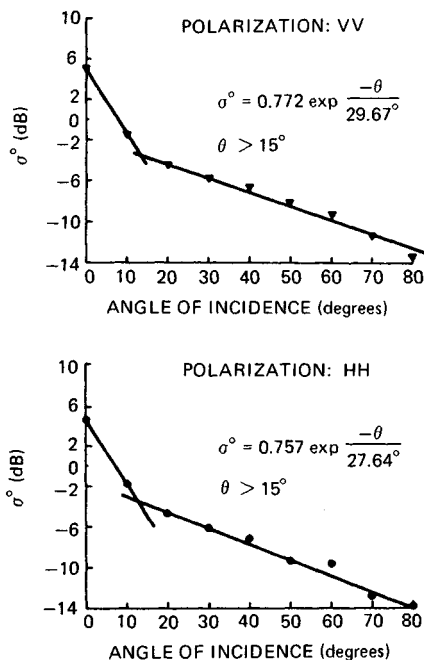


FIG. 12.24 Regression of average of all 1974 and 1975 13.8-GHz cropland data obtained with a microwave active spectrometer. (From Moore, Soofi, and Purduski.⁸²)

frequency, the frequency response shown in the model depends entirely on the MAS measurements.

The summer Skylab observations included deserts, grassland, cropland, and forests, whereas the Kansas measurements were only of cropland. However, early and late in the growing season the cropland was essentially bare, similar to the summer desert except for soil moisture content. During the height of the growing season the crops were dense enough so that scatter was similar to that from forests. Thus, the overall model seems representative of summer conditions averaged over all of North America.

The model takes the form

$$\sigma_{dB}^0(f, \theta) = A + B\theta + Cf + Df\theta \quad 20^\circ \leq \theta \leq 70^\circ \quad (12.24a)$$

where A , B , C , and D take on different values for different polarizations and above and below 6 GHz. The frequency response below 6 GHz is much more rapid than above 6 GHz. Moreover, at frequencies above 6 GHz the frequency response is independent of angle, so that $D = 0$. For lower frequencies, the frequency response is angle-dependent.

For angles less than 20° , only two points were available, 0° and 10° ; so separate frequency regressions were run at each of these angles. The model for these angles is

$$\sigma_{dB}^0(f, \theta) = M(\theta) + N(\theta)f \quad \theta = 0^\circ, 10^\circ \quad (12.24b)$$

The frequency responses below 6 GHz differed for the two years; so the models have separate values of the constants for 1975 and 1976. The year 1976 was very dry in Kansas; so the 1975 values are probably more representative, but both are given here. Values of the constants are in Table 12.2. Figure 12.25 shows the clutter model for the midrange of angles as a function of frequency. The figure is only for vertical polarization because results are so similar for vertical and horizontal.

Ulaby developed a different, more complex model from the Kansas vegetation data.⁸⁵ This model fits curves rather than straight lines to the measured data. For most purposes the straight-line model is adequate, and it is much easier to use.

A straight-line model for snow-covered grassland similar to that for vegetation depends on a more limited data set.^{86,87} The data was for only one season in Colorado when the snow was only about 50 cm deep. This means that the signal probably penetrated to the ground surface at frequencies below about 6 GHz. Nevertheless, the model indicates the kind of results to be expected for this important situation. Table 12.3 gives the resulting constants to use in Eq. (12.24a).

Snow scatter depends strongly on the free-water content of the upper layer of snow; so scatter is much lower from the wet daytime snow (where solar melting has commenced) than for the dry nighttime snow. Hence, different models must be used for day and night; compare the day and night measurements shown in Fig. 12.26. The difference between day and night scatter from snow is even more pronounced at 35 GHz, but the model does not include 35 GHz because no data exists between 17 and 35 GHz.

Although no specific clutter model has been developed for forest, results from the Skylab RADSCAT and Seasat scatterometer show that the Amazon rain forest scatters almost independently of the angle of incidence even near vertical.⁸⁸ The mean measured value at 33° was -5.9 ± 0.2 dB at 13.9 GHz. Observations with SIR-B indicated that this lack of angular variation of σ^0 also is present at 1.25 GHz, but lack of calibration prohibited learning the level of scatter at this frequency.

TABLE 12.2 Constants for Linear Scattering Model (Summer)*

Eq.	Polarization	Angular range, °	Frequency range, GHz	Constant A or M, dB	Angle slope B or N, dB	Frequency slope C, dB/GHz	Slope correction D, dB/(° · GHz)
12.24a	V	20-60	1-6 (1975)	-14.3	-0.16	1.12	0.0051
	V	20-50	1-6 (1976)	-4.0	-0.35	-0.60	0.036
	V	20-70	6-17	-9.5	-0.13	0.32	0.015
	H	20-60	1-6 (1975)	-15.0	-0.21	1.24	0.040
	H	20-50	1-6 (1976)	-1.4	-0.36	-1.03	
	H	20-70	6-17	-9.1	-0.12	0.25	
12.24b	V and H	0	1-6 (1975)	7.6	...	-1.03	
	V and H	0	1-6 (1976)	6.4	...	-0.73	
	V and H	0	6-17	0.9	...	0.10	
	V and H	10	1-6 (1975)	-9.1	...	0.51	
	V and H	10	1-6 (1976)	-3.6	...	-0.41	
	V and H	10	6-17	-6.5	...	0.07	

*After Moore, Soofi, and Purduski.⁸²

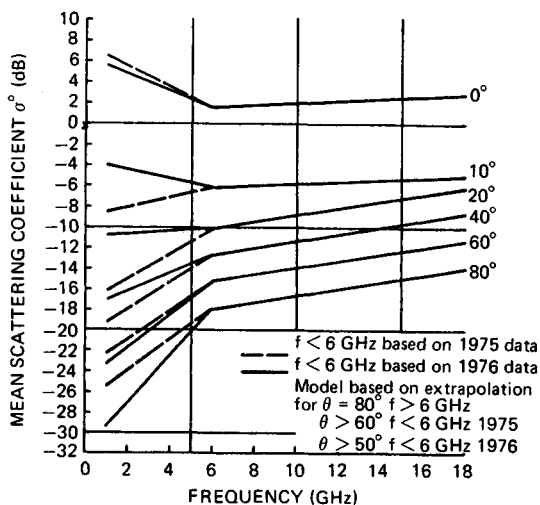


FIG. 12.25 General land-scattering-clutter model (vertical polarization). Horizontal polarization is very similar. (From Moore, Soofi, and Purduski.⁸²)

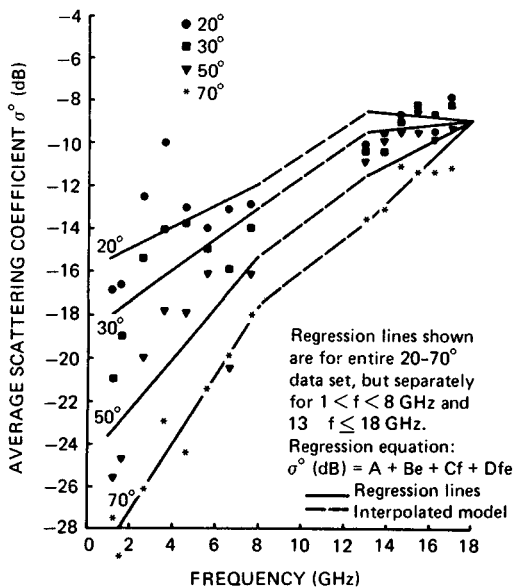
TABLE 12.3 Regression Results for Ground-Based Measurements of Snow-Covered Ground*

Time of day	Polarization	Frequency	Constant A, dB	Angle	Frequency	Slope correction D, dB/ (° · GHz)
		range, GHz		slope B, dB/°	slope C, dB/ GHz	
Day	V	1-8	-10.0	-0.29	0.052	0.022
Day	V	13-17	0.02	-0.37	-0.50	0.021
Day	H	1-8	-11.9	-0.25	0.55	0.012
Day	H	13-17	-6.6	-0.31	0.0011	0.013
Night	V	1-8	-10.0	-0.33	-0.32	0.033
Night	V	13-17	-10.9	-0.13	0.70	0.00050
Night	H	1-8	-10.5	-0.30	0.20	0.027
Night	H	13-17	-16.9	-0.024	1.036	-0.0069

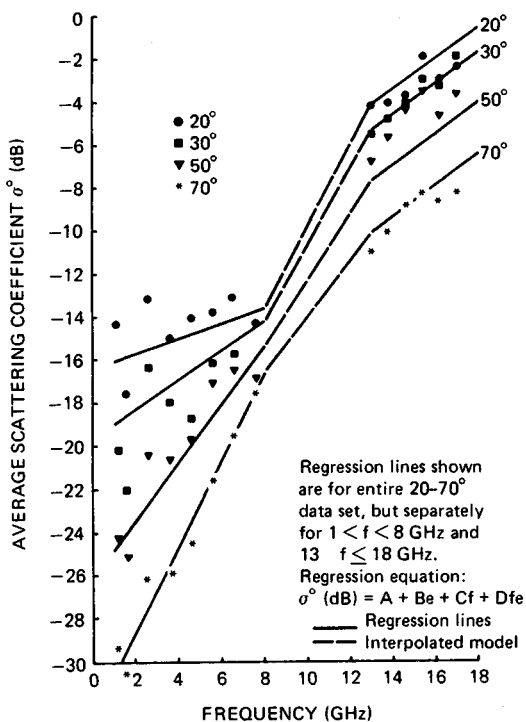
*After Moore, Soofi, and Purduski.⁸²

NOTE: $\theta = 20$ to 70° . Values of coefficients in this table also are considered those of the model.

The models described above are based on averages over very large areas. For this situation the variability from place to place is small, particularly in the midrange of angles. Figure 12.27 shows the mean and upper and lower decile values measured by the Skylab RADSCAT over North America. The larger variation near vertical apparently results from the effect of nearly specular reflection from water bodies. When the footprint is smaller, more variability occurs. This is shown in Fig. 12.28 from a study of the variation of scatter observed by SIR-B



(a)



(b)

FIG. 12.26 Regressions for vertical-polarization clutter model for snow: (a) day and (b) night. Note the large differences. Horizontal polarization is similar. (From Moore, Soofi, and Purduski.⁸²)

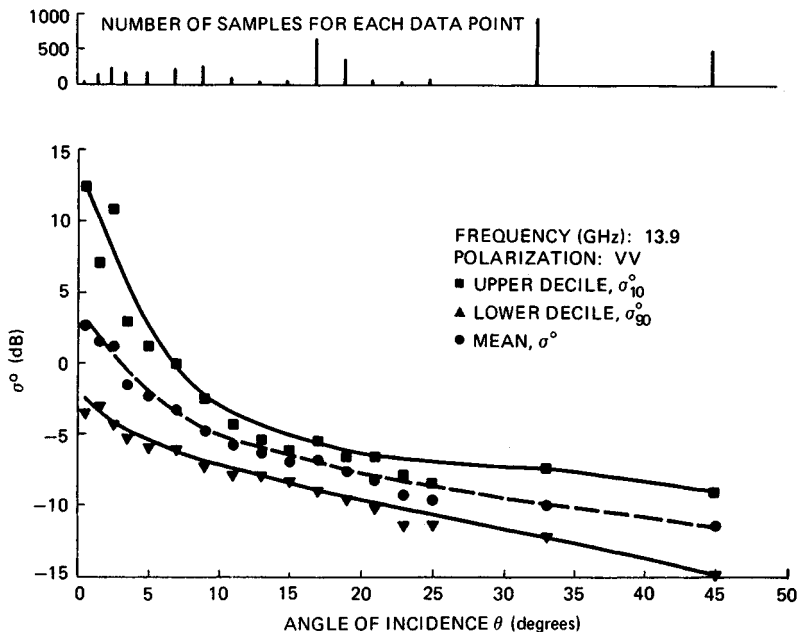


FIG. 12.27 Angular patterns of the mean, upper decile, and lower decile of Skylab scatterometer observations over North America during the summer season. (From Moore et al., University of Kansas Remote Sensing Laboratory Technical Report 243-12, 1975.)

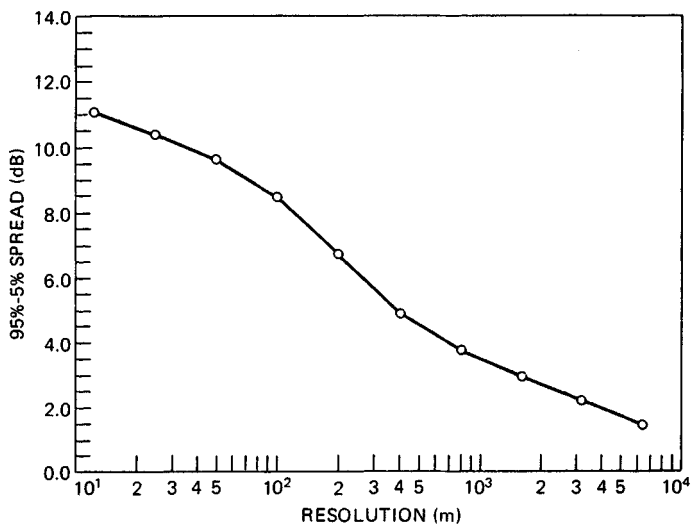


FIG. 12.28 90 percent range of pixel amplitude versus resolution.

with averages over different-sized footprints. For small footprints the scatter varies over a wide range, and system designers must account for this.

12.7 SCATTERING COEFFICIENT DATA

Numerous programs to gather scattering coefficient data existed prior to 1972, but sizable data collections with accompanying "ground truth" were rare. Since 1972, however, several major programs have changed the situation so that much information is now available. Indeed, this information is so widespread that an adequate summary of the literature is impossible. Hence, this section can only give highlights of the results and major programs. The reader should consult the three major compendia of such data for more information both on results and on bibliography^{21,23,114} (note that information is spread through many chapters).

Some early scattering-coefficient-measurement programs worth mentioning include those of the Naval Research Laboratory,^{15,16} Goodyear Aerospace Corporation,¹² Sandia Corporation (near-vertical data),^{89,90} and particularly Ohio State University.^{2,4} Since 1972 the largest program has been at the University of Kansas.^{6,7,21,53,57,69,91} Extensive programs were also in France (Centre National d'Etudes Spatiales, Centre National d'Etudes des Télécommunications, Université Paul Sabatier),⁹ the Netherlands,⁸ Canada Centre for Remote Sensing (CCRS; especially sea ice),¹⁷ and the University of Bern, Switzerland (snow).⁹² Many of the results from these programs appear in digests of the International Geoscience and Remote Sensing Symposia (IGARSS; IEEE Geoscience and Remote Sensing Society) and journals such as *IEEE Transactions on Geoscience and Remote Sensing* and *on Ocean Engineering, International Journal of Remote Sensing, Remote Sensing of Environment, and Photogrammetric Engineering and Remote Sensing*.

Although calibrations for some of the older data were doubtful, summary presentations are not available for newer data. Accordingly, Fig. 12.29 shows an earlier summary based mostly on X-band data. One should be cautious in using this data, but the figure gives a feel for the overall variations. Figure 12.30 is a similar presentation for near-vertical data.⁹³ Calibration of the systems was good, but the antenna effect discussed in Sec. 12.5 makes the values from 0 to 5° low.

Effects of Roughness, Moisture Content, and Vegetation Cover. Scattering falls off more rapidly with angle for smooth surfaces than for rough surfaces. Since the roughness that affects radar must be measured in wavelength units, a surface smooth at long wavelengths may be rough at shorter ones. This is illustrated in Fig. 12.31,⁹⁴ which shows these effects with measurements from plowed fields. At 1.1 GHz the signal changed 44 dB between 0 and 30° for the smoothest field and only 4 dB for the roughest. At 7.25 GHz the smoothest field was rough enough to reduce the variation to 18 dB.

For most surfaces cross-polarized scatter is lower than like-polarized, often by about 10 dB. Cross-polarized scatter from smooth surfaces is much less near vertical than elsewhere. Figure 12.32⁹⁵ shows this effect. Cross-polarized returns from volume scatterers with elements that are large compared with a wavelength are stronger than for surfaces, sometimes being only 3 dB down.

Scatter depends on dielectric constant, which depends on moisture content. Thus scatter from wet soils at angles off vertical is usually much higher